Current Eye Research
1999, Vol. 19, No. 1, pp. 41–52

0271-3683/99/1901-0041 $15.00

Model of human refractive error development

George K. Hung[1] and Kenneth J. Ciuffreda[2]

[1]Department of Biomedical Engineering, Rutgers University, 617 Bowser Road, Piscataway, N.J. 08854-8014, USA; [2]Dept. of Vision Sciences, State College of Optometry, State University of New York, 100 E. 24th St., New York, NY 10010, USA

Abstract

Purpose. To construct a model of refractive error development that can account for the different interactive mechanisms and time courses of refractive error in the hyperope (HYP), emmetrope (EMM), early-onset myope (EOM), and late-onset myope (LOM) over the first 30 years of life.

Methods. First, a baseline short-term (1 mo.) simulation of a previously developed nearwork-induced transient myopia (NITM) model was performed under both far- and near-viewing paradigms to obtain the critical relationships between AE_{rms} and refractive error for the four refractive groups. Then, two control pathways were added to the NITM model. The genetically-controlled pathway was associated with the long-term growth of the cornea, lens, and the eyeball. The environmentally-controlled pathway was associated with retinal-defocus during nearwork, wherein the root mean square (rms) of the accommodative error (AE) above a threshold level resulted in an increase in axial length of the eyeball. The thresholds for defocus-induced axial length change were empirically determined to correspond to the differential susceptibility in the four refractive groups. The combination of effects from the two pathways produced the overall refractive error. The relationship between AE_{rms} and refractive error was combined with the two control pathways for the long-term simulations (30 yrs: the initial 15 yrs using a far-viewing paradigm followed by an additional 15 yrs using a near-viewing paradigm) to quantify refractive error development as related to daily nearwork activity in the four refractive groups.

Results. All refractive groups began early in life with a genetically-determined hyperopic refractive error. The HYP had the lowest susceptibility or highest threshold to retinal defocus effects, and remained at a hyperopic level. The EMM exhibited a relative myopic shift in the first 2 years to become and remain at emmetropia. In the myopic groups, the EOM exhibited both a genetically-controlled component (starting 2 years of age) and a defocus-induced component (starting at 15 years of age), whereas the LOM manifested only a defocus-induced factor (starting at 15 years of age) in the development of myopia. In addition, simulations indicated that emmetropization occurred only for "induced" refractive error that was less than 0.5 D, which was consistent with the non-monotonic relationship between AE_{rms} and refractive error, wherein the minimum AE_{rms} occurred at 0.5 D.

Conclusions. The model showed that both genetic and defocus-induced environmental factors play important roles in the development of refractive error in the different refractive groups. The model also provides a framework for further detailed quantitative analysis of the processes of refractive error development and emmetropization.

Keywords: *human refractive error development*; emmetropization; myopia; accommodation; *control systems model*

Introduction

If the cornea and lens grow perfectly in concert with the scleral tunic during the ocular growth and development phase, there would be an exact match between the refractive (i.e., optical) and mechanical (i.e., ocular tunic) components of the eye. Hence, a difference in their growth patterns will lead to a refractive error. Thus, genetic control (1) of ocular growth plays an important role in the emmetropization process, as well as the overall development of refractive error. In addition, environmental factors, such as nearwork, have been shown to produce a deviation from the emmetropic growth pattern with the consequent development of refractive error, in particular in late-onset myopia (see reviews by Ong and Ciuffreda (2, 3)). Moreover, differences in individual susceptibility to potential nearwork effects add to the complex

Correspondence: George K. Hung, Department of Biomedical Engineering, Rutgers University, 617 Bowser Road, Piscataway, N.J. 08854-8014, USA, Tel: (732) 445-4137, Fax: (732) 445-3753, E-mail: shoane@rci.rutgers.edu

Received on November 12, 1998; revised on January 25 and accepted on February 24, 1999

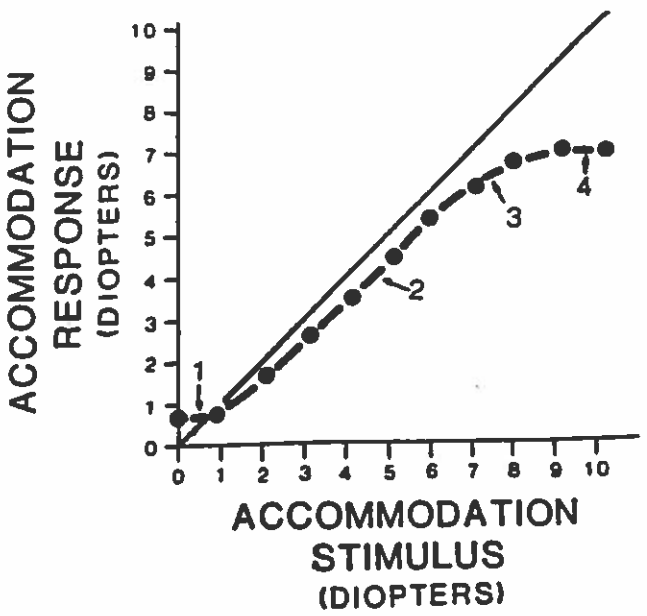

Figure 1. Schematic representation of the static accommodative stimulus-response curve for a typical normal subject. 1 = initial non-linear portion, 2 = linear region, 3 = transitional soft saturation region, and 4 = hard saturation region. Adapted from Ciuffreda and Kenyon (9) permission from the authors.

interplay between genetic and environmental factors in myopia development. For example, young-adult myopes are more susceptible to nearwork accommodative aftereffects than either emmetropes or hyperopes (4). Therefore, understanding the underlying mechanisms of myopia development and eventually its prevention has been of considerable interest in recent years (5, 6).

Due to the control properties of the accommodation system and the extent of the ocular depth-of-focus, the accommodative response is typically less than the accommodative stimulus for near viewing (i.e., the lag of accommodation), so that the retinal image is normally focused slightly behind the retina (7, 8) (Fig. 1). Also, as the accommodative stimulus increases, the accommodative error and resultant retinal defocus increase proportionally (7–9). Recent evidence in animals has shown that during ocular development, the eye grows in the direction of the induced retinal-image defocus (10, 11). This suggests that the eye may either elongate or decrease in its growth rate in response to the resultant defocused retinal-image as part of the emmetropization process (i.e., the tendency for ocular growth towards emmetropia) (12). Blur-induced biochemical factors appear to play a primary role in causing local scleral growth (13), as such elongation occurs even when the optic nerve is severed. Moreover, a recent study using partial coherence interferometry revealed only a very small ciliary muscle-induced increase in axial length during accommodation (14), which appears to be below the threshold for inducing growth, thus discounting any major role played by the direct mechanical effects on the sclera (3). Furthermore, there is evidence that children who become myopic have relatively inaccurate and reduced steady-state accommodative response at near to blur-only stimuli (15). Thus, it appears there are two primary paths in ocular refractive development, one associated with genetically-based normal growth of the refractive elements and the ocular tunic, and a second associated with the environmentally-based contribution of local retinal-image defocus, which causes deviation from normal growth and emmetropia.

Several models related to refractive error development and emmetropization have been proposed. Schaeffel and Howland (16) introduced a model that separated the optical and retinal-defocus processes. They suggested that the experimental data obtained in chickens could be described by processes containing two such feedback loops. One loop was dependent on lens response feedback, and the other was dependent on retinal-image feedback. They also presented model simulation fits to some of their experiment data. Medina (17) proposed a model of emmetropization in humans using an equation composed of the sum of a genetically-determined refractive state term and a group of terms each consisting of the product of an exponential and a cosinusoid (thus providing decaying-oscillatory signals at different time shifts). This model was used to fit experimental data on refractive error as a function of age. The results suggested that wearing corrective lenses would increase the existing ametropia. However, since the model did not actually include an accommodative feedback component for viewing over various distances, the refractive error could not be reduced by the normally-present visual feedback mechanism. Hence, in essence the refractive error was forced to increase with the introduction of corrective lenses. Clearly, this model does not accurately represent the human emmetropization process during lens wear. More recently, Flitcroft (18) introduced a model of emmetropization and myopia in humans based on the dual-interactive model of Hung and colleagues (19–21). He proposed an integrative measure of accommodative error that was dependent on the accommodative stimulus, refractive error, and the amount of time spent at nearwork and at farwork. This aggregate measure was used to update the refractive error at each iterative loop in the model simulation by subtracting the product of this integral measure and the emmetropization gain from the previous refractive error value. He also presented simulations of the effect of nearwork on increased final refractive error. However, no explicit genetic control factors or thresholds that accounted for refractive-based differential susceptibility in the various refractive groups were used. Blackie and Howland (22) extended Flitcroft's model to include pupil size effects.

To provide a more comprehensive analysis of these genetic and retinal-defocus interactions for the different refractive states, as well as demonstrate the process of emmetropization, a new comprehensive model of human refractive error development was conceptualized and tested using a control systems approach.

Methods

Model

A descriptive block diagram of the model is shown in Fig. 2A. The basic loop is essentially the same as a recently proposed and tested nearwork-induced transient myopia (NITM) model (23). It consists of the conventional accommodative feedback loop in which the accommodative error (AE) drives the accommodative controller and then the lens plant. The accommodative response (AR) is fed back and then subtracted from the accommodative stimulus (AS) to provide an updated accommodative error (i.e., AE = AS – AR). For simplicity, the adaptive and proximity components of the NITM model are not shown in this descriptive figure, but will be described in more detail in Fig. 2B.

Two interactive paths, the genetically- and environmentally-controlled pathways, were added to the NITM model. The genetically-controlled long-term growth element (normal or abnormal) drives the cornea/lens complex, as well as the axial length components. The retinal defocus-induced change in axial length from the environmentally-controlled pathway is added to that from the genetically-controlled pathway to result in the total axial length. Then, the cornea/lens value from the genetically-controlled pathway is converted to total ocular power for far viewing, and the total axial length is converted to total axial length equivalent power. The difference between the total ocular power at far and the total axial length equivalent power represents the refractive error (Fig. 2B). Finally, this refractive error value is subtracted from the target accommodative stimulus to provide the accommodative error to drive the accommodation system. Thus, for a myopic refractive error, this positive value would be subtracted from the target accommodative stimulus (by convention, positive for stimulating accommodation) to provide

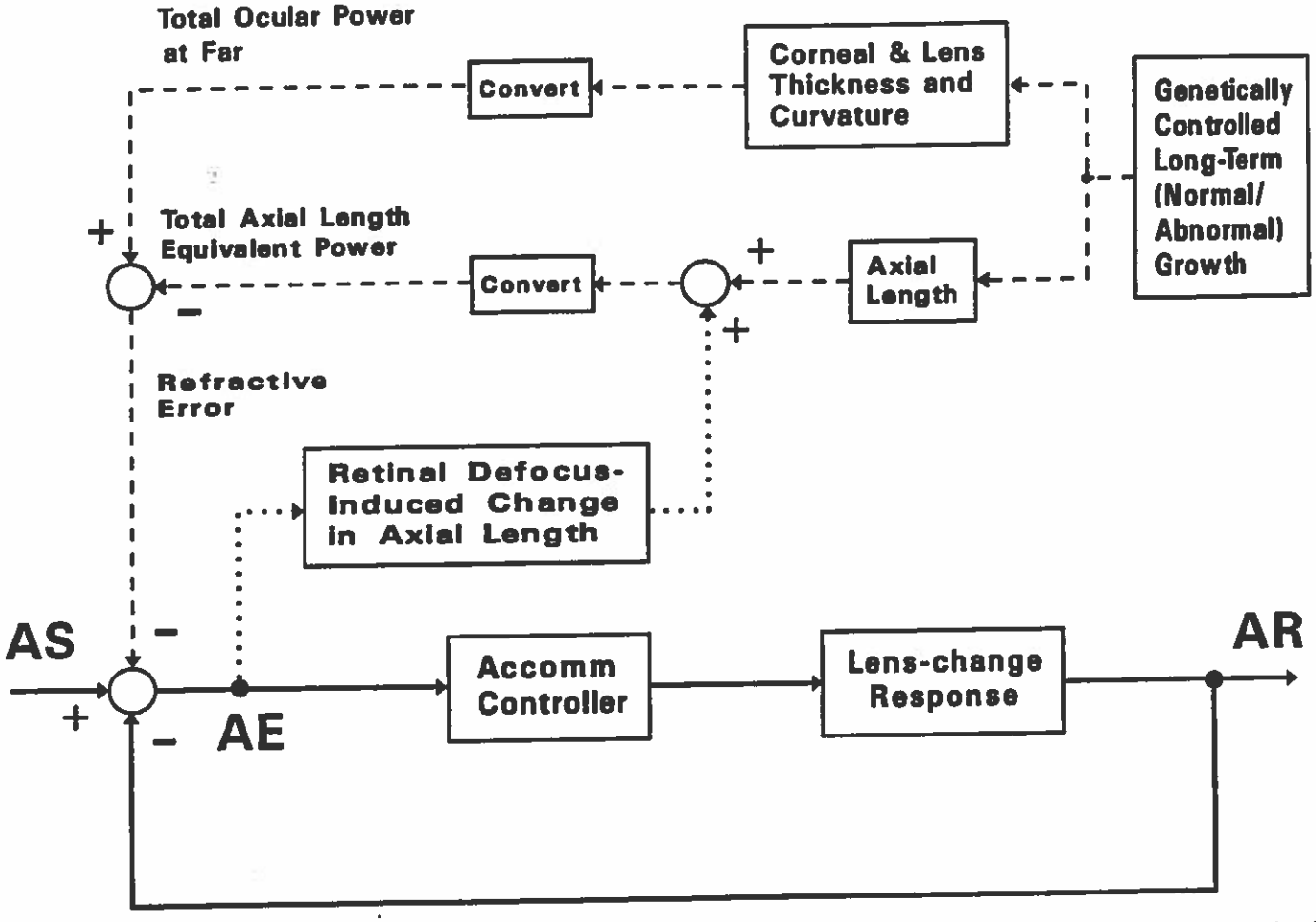

Figure 2A. Descriptive block diagram of refractive error development model. The basic model (solid lines) consists of the conventional accommodative feedback loop where the accommodative error (AE), equal to the accommodative stimulus minus the accommodative response (or AS - AR), is input to the accommodative controller whose output drives the lens to provide the AR. In addition, this model contains signals from the axial length component of the genetically-controlled pathway (dashed lines) and the retinal-defocus (AE) induced environmentally-controlled pathway (dotted lines) that sum to provide the total change in axial length. This is converted to total axial length equivalent power and is subtracted from the total ocular power at far (due to combined lens and corneal powers from the refractive component of the genetically-controlled pathway, dashed lines) to provide the overall refractive error. The refractive error is then fed back and added to AS to provide the total accommodative stimulus for driving the feedback loop.

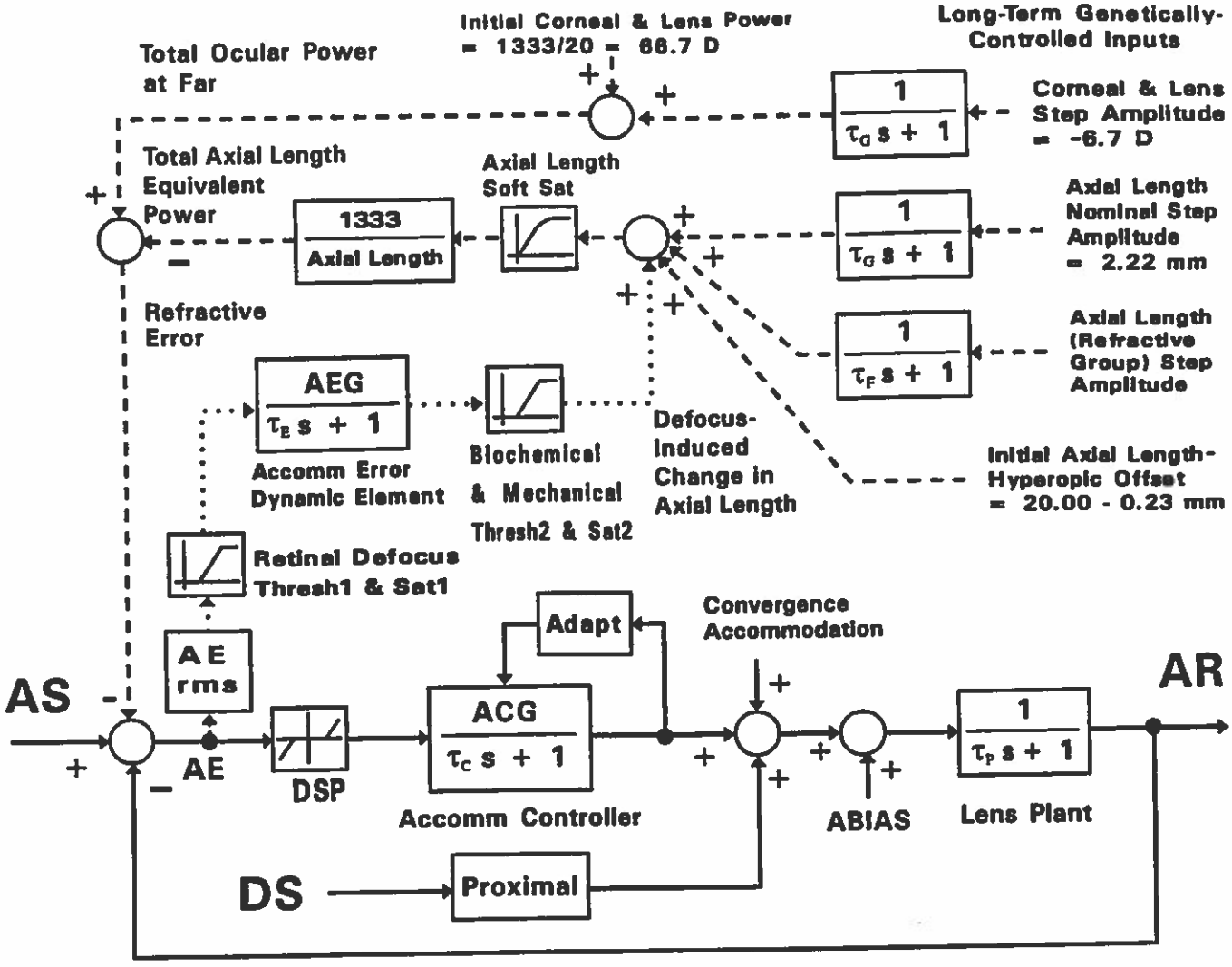

Figure 2B. Detailed block diagram model of refractive error development model. See text and Table 1 for details.

the actual stimulus to accommodation. For example, a target 20 cm (5 D) in front of a 2 D uncorrected myope would result in a 3 (= 5–2) D accommodative stimulus. On the other hand, for a 2 D uncorrected hyperope, the net accommodative stimulus would be 7 (= 5+2) D.

A more detailed, quantitative version of this model is shown in Fig. 2B. In the basic accommodative loop, a deadspace element representing the depth-of-focus (± DSP) is added in front of the accommodative controller, which is represented by a dynamic element with gain ACG. The values of ACG for the different refractive groups were derived from previously-obtained accommodative stimulus/response slope measures (24) using the equation ACG = slope/(1-slope) (25), but with an upper limit for ACG of 21 to preclude instability feedback oscillations (26). The time constants, τ_C and τ_P, represent the speed of response of the accommodative controller and the plant, respectively (27, 28). Other components added to the basic loop include the proximal (perceived distance gain, PDG; accommodative proximal gain, APG; vergence proximal gain, VPG) and adaptive elements (accommodative adaptation gain, K_A (for simplicity not shown in Fig. 2B); vergence adaptation gain, K_V), crosslink gains (accommodative convergence gain, AC; convergence accommodation gain, CA), and tonic terms (tonic accommodation, ABIAS; tonic vergence, VBIAS). The proximal component values were obtained from a previously-derived proximal model (21). The K_A values were different for the various refractive groups to simulate differences in their NITM time courses (23). Further, the ABIAS values for the different refractive groups were obtained from a study by McBrien and Millodot (29) (see Table 1).

The genetically-controlled pathway (Fig. 2A) provides the drive for both the cornea/lens complex and axial length growth. The experimental data for normal axial length growth consisted of two parts: an initial phase that grew rapidly to about 20 mm, and a second phase that grew more slowly, reaching a length asymptotically that corresponded to emmetropia (30). For simplicity, the very rapid early growth phase to about 20 mm was simulated by an initial axial length of 20 mm, and the subsequent growth to 22.22 mm (corre-

Table 1. Summary of model parameter values

Path	Parameter	Parameter values for four refractive groups HYP	EMM	EOM	LOM
Normal visual feedback loop pathway	Accomm. Deadspace, ± DSP (D)	± 0.15	± 0.15	± 0.15	± 0.15
	Vergence Deadspace, ± DSP (MA)	± 0.012	± 0.012	± 0.012	± 0.012
	Accomm Adaptation Gain, K_A	2.0	2.5	4.0	5.5
	Vergence Adaptation Gain, K_V	10.0	10.0	10.0	10.0
	Perceived Distance Gain, PDG	0.212	0.212	0.212	0.212
	Accomm Proximal Gain, APG	2.10	2.10	2.10	2.10
	Vergence Proximal Gain, VPG	0.067	0.067	0.067	0.067
	Accomm Controller Gain, ACG	21.0	11.5	7.3	6.7
	Vergence Controller Gain, VCG	150.0	150.0	150.0	150.0
	τ_C (sec)	4	4	4	4
	τ_P (sec)	0.3	0.3	0.3	0.3
	Acc. Conv. Gain, AC (MA/D)	0.80	0.80	0.80	0.80
	Conv. Acc. Gain, CA (D/MA)	0.37	0.37	0.37	0.37
	Tonic Accomm or ABIAS, (D)	1.35	0.80	0.85	0.45
	Tonic Vergence or VBIAS, (MA)	0.29	0.29	0.29	0.29
Long-term genetic	Axial Length (Refractive Group)				
	Step Amplitude (mm)	–0.33	0.23	1.85	0.23
	τ_F (yr)	2	2	5	2
	τ_G (yr)	2	2	2	2
and environmental (retinal-defocus) pathway	Accomm. Error Gain, AEG	10	10	25	9
	τ_E (yr)	2	2	2	1
	Thresh 1 (D)	0.40	0.40	0.35	0.20
	Sat 1 (D)	0.02	0.02	0.02	0.02
	Thresh 2 (mm)	0.10	0.10	0.10	0.01
	Sat 2 (mm)	1.0	1.0	1.0	1.0

sponding to 1333/22.22 = 60 D) was simulated by the addition of a step input of axial- length growth with an amplitude of 2.22 mm a time constant, τ_G, of 2 years (Fig. 2B). To complement this normal axial length growth, the corneal and lens growth was also divided into two parts, with an initial power equal to 1333/20 = 66.7 D, and the subsequent return to 60 D was simulated by the addition of a corneal and lens step of ocular power with an amplitude of –6,7 D and a time constant, τ_G, of 2 years. The above conditions would have produced emmetropia throughout its time course. However, to account for the hyperopia that is seen in the early years of life (31–34), a –0.23 mm step input of axial-length change (equivalent to –0.75 D of hyperopia for an initial 20 mm axial length; see Eq. 1 below) was added (see Fig. 2B). Also, to simulate the various refractive conditions, different step inputs of axial-length change with time constant, τ_F, were added to the axial length growth component. For HYP, EMM, EOM, and LOM, the step amplitudes and time constants were -0.33 mm and 2 yrs, 0.23 mm and 2 yrs, 1.85 mm and 5 yrs, and 0.23 mm and 2 yrs, respectively (see Table 1). Subsequent defocus-induced changes in axial length were dependent on the threshold and saturation values in the long-term closed-loop simulation of refractive error development using the look-up table (not shown explicitly in Fig. 2B, but would effectively replace the lower feedback loop to provide a link between refractive error and AE_{rms}) for AE_{rms} versus refractive error (Figs. 4A, B). The final steady-state refractive errors for HYP, EMM, EOM, and LOM of -1.5 D, 0 D, 5 D, and 1.5 D, respectively, were consistent with mean values obtained experimentally (4).

On the other hand, in the environmentally-controlled pathway, the root mean square (rms) of the accommodative error (AE) is detected by a retinal-defocus element. AE_{rms} is an expression that represents the square root of the sum of all the squared values of AE over the measured time interval divided by the number of time samples. Because it is a squared-value measure, it is insensitive to the sign of AE. The output of this element is then input to the accommodative error dynamic element with gain AEG, which is associated with the relatively long timecourse (i.e., months or even years) needed for producing the retinal defocus-related biochemical and mechanical changes in the ocular tunics. The time constant of this biochemical and mechanical process is given by τ_E (Table 1). Both this retinal-defocus element, as well as the subsequent biochemical and mechanical elements, have threshold and saturation components. Thresholds are important for distinguishing between the different refractive groups and represent a measure of the susceptibility to change in axial length, as they determine the amount of retinal defocus necessary to activate the blur-based environmental process. Also, small errors that are not above the threshold will not accumulate over time

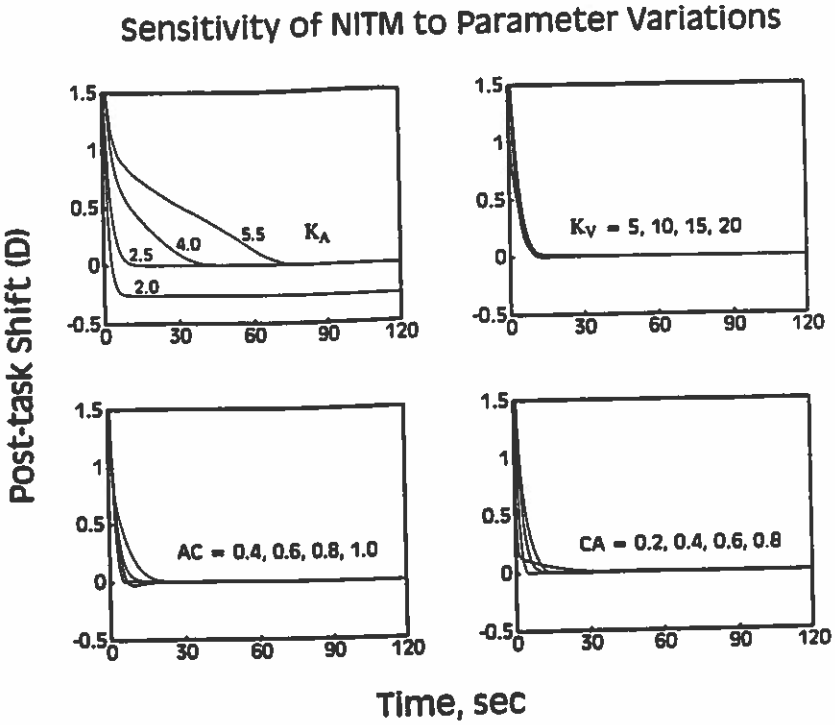

Figure 3A. Sensitivity analysis of NITM to variations in the parameters for K_A, K_V, AC, and CA, showing greater sensitivity for K_A than the other parameters.

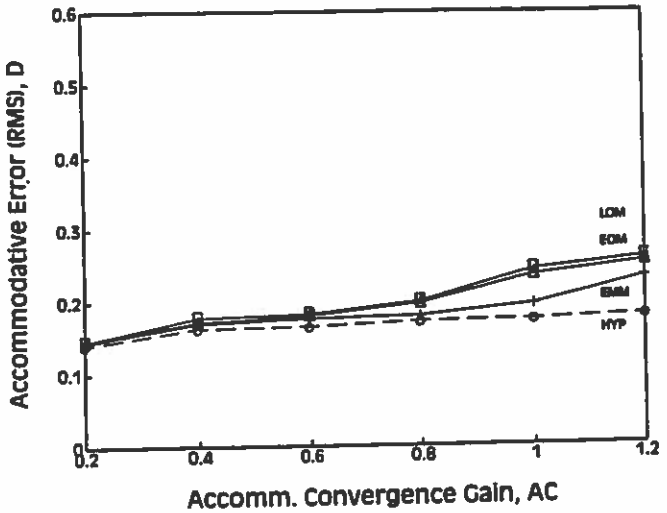

Figure 3B. Sensitivity analysis of (160 hrs) nearwork AE_{rms} to variation in accommodative convergence crosslink gain, AC, showing relatively low sensitivity to changes in AC for the four refractive groups. Compare with Figs. 4A, B.

to become large errors. In contrast, the saturation components set the upper limits to the output of these processes. The output of the dynamic element is added to the genetically-controlled axial length component to result in the total axial length. This is input to a soft (i.e., gradual rather than abrupt) saturation element to limit the extent of axial elongation, and its output is then converted to equivalent optical power. The genetically-controlled corneal and lens components are also converted to an equivalent optical power. The difference between these two equivalent optical powers results in the overall measured refractive error. That is, if the normal corneal and lens growth is balanced by normal axial length growth, no refractive error will develop, and emmetropia will be attained. On the other hand, if prolonged exposure to suprathreshold retinal defocus results in an increase in axial length, this will produce an effective or relative decrease in total axial length equivalent power. Therefore, if the difference between the total ocular power at far and the total axial length equivalent power is positive, indicating the eye is optically too powerful, then myopia will develop. The exponentially-shaped dynamic time courses of refractive error change were based on experimental data obtained during the early (31, 35) and later years of life (32).

Simulations

The present model simulations were based on and are extensions of the previous NITM model study (23). First, to assess the effect of variations in the model parameters on the NITM time course, accommodative as well as vergence parameters were varied. Accommodative parameters included accommodative adaptation gain (K_A), accommodative controller gain (ACG), accommodative convergence crosslink gain (AC), and tonic accommodation (ABIAS). Vergence parameters included vergence adaptation gain (K_V), vergence controller gain (VCG), convergence accommodation crosslink gain (CA), and tonic vergence (VBIAS). For simplicity, the

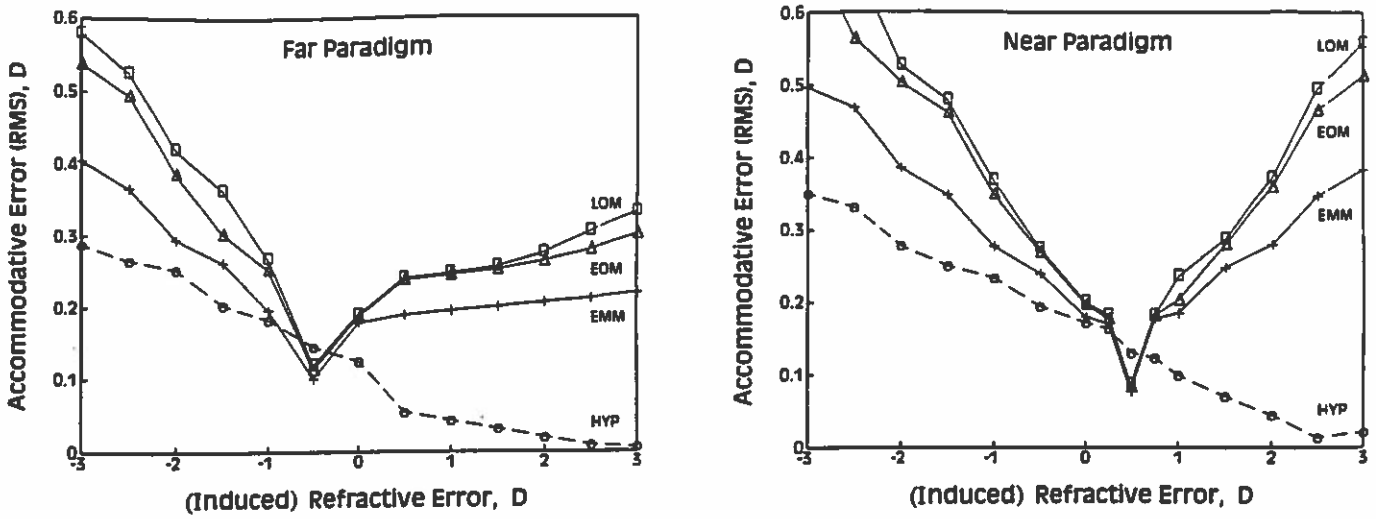

Figure 4. AE_{rms} versus "induced" refractive error for the four refractive groups under the (A) FAR and (B) NEAR paradigms. These data were stored as look-up tables in the form of SIMULINK blocks (not shown in Fig. 2B) and used in the long-term (30 yrs) simulations.

vergence loop was not shown in Figs. 2A, B but their contributions were included in the convergence accommodation term. The deadspace operator was simulated by the following algorithm: if input > DSP, then output = input-DSP; otherwise, if input < -DSP, then output = input + DSP; otherwise, output = 0. A 4th-order Runge-Kutta algorithm was used to integrate the 1st-order dynamic terms of the form $1/(\tau_C s + 1)$, where τ_C is the controller time constant (see Table 1). The NITM paradigm consisted of 10 min of near viewing at 5 D and 5 MA, with this being followed by 2 min at 0.17 D and 0.17 MA in which the transient myopia is measured. The results were plotted to provide an assessment of the sensitivity of NITM to variations in each of the parameters. In addition, a sensitivity analysis was performed to assess the effect of variation in accommodative convergence crosslink gain, AC, on accommodative error, under a nearwork (NEAR) paradigm (see below). The results were plotted as AE_{rms} versus AC for the four refractive groups.

Second, AE_{rms} was obtained for different "induced" refractive errors under the FAR and NEAR viewing paradigms. The term "induced" refractive error is used here to indicate that it is effectively equal to the placing of lenses in front of the eyes, which should be distinguished from the actual refractive error per se of a refractive group. Moreover, throughout these simulations, it is assumed that the refractive groups have been corrected with lenses as needed, and that variations among the groups are due to differences in their internal model parameter values. In the FAR paradigm, the stimulus consisted of a repeated sequence of 1 hr of congruent far (0.25 D and 0.25 MA) and 5 min of near (3D and 3 MA) viewing for 160 hrs (equal to a work-month). On the other hand, in the NEAR paradigm, the stimulus consisted of a repeated sequence of 1 hr of congruent near (3 D and 3 MA) and 5 min of far (0.25 D and 0.25 MA) viewing for 160 hrs. The "induced" refractive error was varied from –3 to 3 D in 0.5 D increments for each of the refractive groups. For each "induced" refractive error value, the AE_{rms} was measured following the 160 hr interval. The results were plotted (Fig. 4A, B) and also put in a look-up table form (with linear interpolation as a SIMULINK block; not shown explicitly in Fig. 2B) for use in the long-term simulations.

Following these relatively short-term simulations, the long-term (30 yrs) simulations were performed using the genetically- and environmentally-controlled pathways, along with the look-up table for the relationship between AE_{rms} and refractive error that replaced the lower feedback loop in Fig. 2B. Two viewing paradigms were used: the FAR paradigm for ages up to 15 years; and the NEAR paradigm for ages 15 to 30 years. Such a separation in viewing paradigms is somewhat arbitrary, but it is primarily based on the previously established transition at age 15 years between early- and late-onset myopia (12). The rationale for assuming a predominantly genetic drive during the earlier years is that children do relatively little nearwork, and thus the development of EOM is most likely due to genetic factors. On the other hand, after age 15 years, during high school and college, a substantially greater amount of nearwork is performed, and thus LOM can be attributed primarily to retinal-defocused induced factors.

In the environmentally-controlled pathway, the AE_{rms} value from the look-up table in the SIMULINK block served as the input. On the other hand, for the genetically-controlled pathway, the step signals (ocular power (D) for the corneal/lens complex, and axial length growth (mm) for the axial length component) served as the input (Fig. 2B). These inputs drove the various elements in the long-term pathways, as specified by their respective time constant, gain, threshold, and saturation parameter values (see upper loops in Fig. 2B, dashed and dotted connecting lines; Table 1), to provide the simulated ocular growth over a 30 year period. The difference between total corneal and lens ocular power at far, and the total axial length equivalent power, equaled the overall

refractive error. The refractive error provided the AE_{rms} value via the look-up table, and this completed the long-term feedback loop. In the simulations, the time course of refractive error was recorded and plotted.

In the environmentally-controlled pathway, AE_{rms} was input to the 1st-order dynamic element with accommodative error gain (AEG) time constant (τ_E) (see Table 1). This element was simulated using a standard SIMULINK function block. Also, the elements containing threshold and saturation (Thresh1 and Sat1, and Thresh2 and Sat2) were simulated with functions first written as m-files and then converted into simulation blocks. On the other hand, for the genetically-controlled pathway (dashed lines), the corneal/lens power and axial length change inputs drove 1st-order elements (Fig. 2B, Table 1). The conversion from axial length to ocular power was performed by an m-file called Oneover.m (not shown explicitly in Fig. 2B) that took the reciprocal of the input, and this was multiplied by 1333 to compensate for the difference in the index of refraction between air and water (36). Finally, the output from the axial length block was subtracted from the refractive block to provide the overall refractive error. The timecourses for the refractive error as well as defocus-induced axial length change were plotted on a Hewlett-Packard laserjet printer.

The values of certain parameters in the model were obtained using different techniques. In the lower feedback loop used for NITM and the FAR and NEAR paradigms, τ_C was derived by fitting the shape of the simulation curves to accepted experimental data (12, 30, 37–39). In the upper loops used for completing the long-term (30 yrs) simulation, the gain AEG, time constant τ_E, and the threshold parameters in the environmentally-controlled pathway, as well as the gain and time constant of the input dynamic term in the genetically-controlled pathway, were all obtained empirically via a trial and error procedure, starting with nominal values and varying each parameter individually while holding the remaining parameters fixed during the simulations, until the rms of the difference in the timecourses between model and experimental refractive error development was within 10%. Moreover, the saturation values in the threshold elements were based on preliminary tests and selected so that the AE_{rms} stimulation of axial length growth remained within normal limits (3).

The model simulations were performed on a 450 MHz PC, where a QUICK BASIC program was used for the NITM and the FAR and NEAR paradigms, and a MATLAB/SIMULINK program was used for the long-term (30 yrs) simulation. The MATLAB/SIMULINK program will be made available to any interested investigators, via a request to the corresponding author, to extend the applications of our model and to serve as basis for continued dialogue regarding the quantitative aspects of refractive error development and emmetropization.

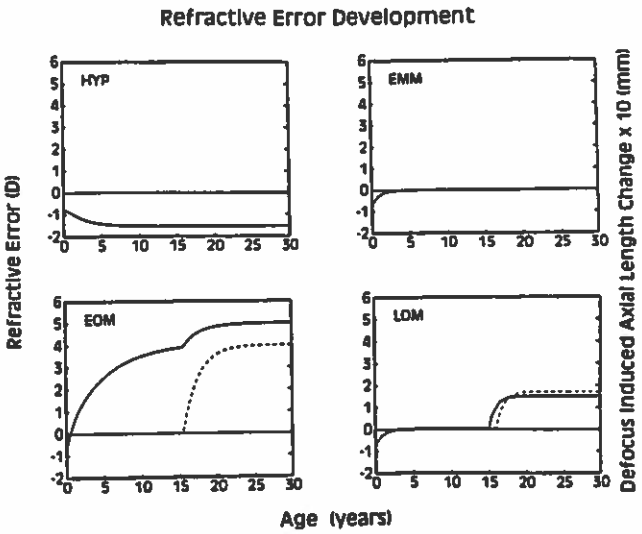

Figure 5. Model simulation results for long-term (30 yrs) development of refractive error (dashed) and retinal defocus-induced axial length change (dotted) in the four refractive groups.

Emmetropization

Emmetropization was demonstrated using the model parameters for the LOM, along with the addition of a square-wave of "induced" refractive error with (arbitrarily selected) peak-to-peak amplitude of 0.5 D and period of 7 years. Two modifications were made in the LOM parameters. The Near paradigm was used throughout the 30 year simulation period, and Thresh1 was reduced from 0.2 mm to 0.1 mm to allow for a fuller range of stimulation. During the first 15 years, the "induced" refractive error was biased by +0.25 D, whereas during the second 15 years, it was biased by –0.25 D.

Relationship between change in ocular power and change in axial length

For a given initial axial length, L (in mm), the change in ocular power ΔP (in D) due to a change in axial length ΔL is given by[36] :

$$\Delta P = \left[\frac{1}{L} - \frac{1}{(L + \Delta L)}\right] * 1333 \qquad (1)$$

Conversely, the change in axial length to provide a change in ocular power is given by

$$\Delta L = \left[\frac{L * 1333}{1333 - L * \Delta P}\right] - L \qquad (2)$$

For example, for an initial axial length of 20 mm, a change in ocular power of 0.75 D would require a change in axial length of 0.23 mm.

Results

The plots of sensitivity of NITM timecourse to variations in the parameters K_A, K_V, AC, and CA are shown in compos-

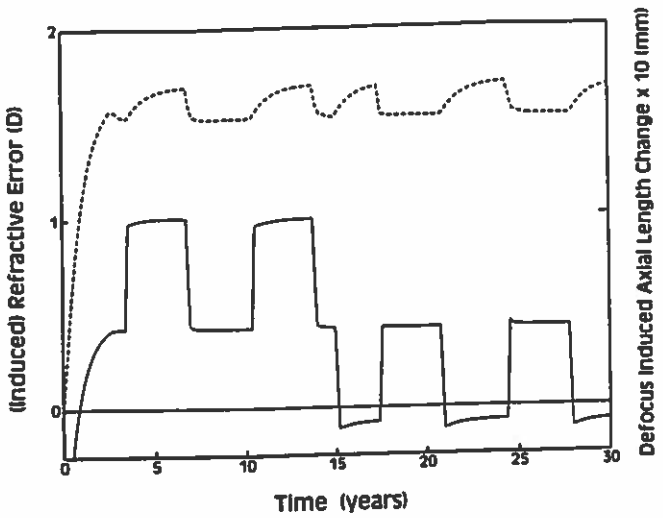

Figure 6. Effect of the addition of a square wave of "induced" refractive error (0.5 D peak-to-peak amplitude and period 7 yrs) (solid) on retinal-defocus induced axial length (dashed) for a complete long-term feedback model of LOM under the Near paradigm over the 30 year interval. Emmetropization is not observed when the stimulus is between approximately 0.5 and 1.0 D during the first 15 years. However, emmetropization can be observed in the reduction in axial length with increased "induced" refractive error when the stimulus is between approximately 0 and 0.5 D during the second 15 years.

ite Fig. 3. It can be seen that NITM is substantially more sensitive to variations in K_A than is true for the other three. Variations in other related parameters (ACG, VCG, ABIAS, and VBIAS) that are not shown in Fig. 3A also exhibited similar insensitivity. Hence, K_A is the most significant parameter in terms of its effect on accommodative error. Also, the plot of the sensitivity of AE_{rms} versus AC for the NEAR paradigm (Fig. 3B) in the four refractive groups showed that accommodative error is relatively insensitive to variations in AC (similar to the flat portion of Fig. 4A). Its effect is evident only for very high AC values, which may explain in part the observed relationship between higher AC/A ratio and myopia development (39). The relationship may also be due to an inherently higher K_A in myopes and the consequent need for higher AC gain to maintain oculomotor balance.

The AE_{rms} versus "induced" refractive error for the different refractive groups is shown for the FAR (Fig. 4A) and NEAR (Fig. 4B) paradigms. Both FAR and NEAR curves exhibit a non-monotonic, V-shape, with the FAR and NEAR curves having minima of "induced" refractive error at approximately –0.5 D and 0.5 D, respectively. The difference between these two minima appear to be associated with their operations on either side of the depth-of-field, or deadspace operator for accommodation (40). Moreover, there is a flattening in the FAR curves for larger "induced" refractive errors, indicating a lack of effect for far viewing. All of these data were input to the appropriate look-up tables for the long-term MATLAB/SIMULINK simulations.

The plots of AE_{rms} versus refractive error (Figs. 4A, B) should be very similar to that found for bifocal ADDs. This is because both paradigms effectively involve the introduction of lenses in front of the subject's eyes. The main difference between our paradigm of "induced" refractive error and the bifocal ADDs is that in our paradigm, the lenses are "worn" at all times, whereas for near bifocal ADDs, the ADDs are not used during far viewing. Also, our paradigm allowed for both plus and minus lenses, whereas for near bifocal ADDs, only plus lenses are used. We are presently investigating the quantitative aspects of near bifocal ADDs, and hence will defer the detailed analysis in a later report.

The parameters determined and used for the long-term simulations are shown in Table 1. It is evident that there are relatively large differences in parameter values, particularly for thresholds and saturation, long term growth gain AEG, and axial length change step amplitude for the different refractive groups (Fig. 2B). The model simulation results for refractive error and retinal defocus-induced axial length change as a function of age for the four different refractive groups are shown in Fig. 5. They indicated that genetic influence was predominant during the first 15 years. All four refractive groups began at about 0.75 D of hyperopia (32). While the hyperopes continued to become more hyperopic, eventually reaching –1.50 D, the other refractive groups showed a genetically-driven myopic shift in the first two years (35, 41), with EMM and LOM (up to age 15 years) attaining emmetropia after these two years. The EOM, on the other hand, continued to exhibit a myopic shift which then leveled off at about 15 years of age. Defocus-induced influences began to show their effect after age 15 years in the myopic groups, with this being the primary drive for LOM. On the other hand, in EOM, the defocus-induced factor was added to the level attained under genetic influence to result in the overall refractive error.

Emmetropization simulation

Emmetropization is not seen during the first 15 years, when the "induced" refractive error is between approximately 0.5 and 1.0 D. Axial length and "induced" refractive error change in the same direction, and thus would be consistent with the progressive increase in axial length with increased retinal defocus that is found in myopia development. On the other hand, the process of emmetropization can be seen during the second 15 years, when the "induced" refractive error is between approximately 0 and 0.5 D. Axial length decreases with increased "induced" refractive error, which is consistent with emmetropization.

Discussion

The model configuration was designed to provide an accurate conceptualization and quantitation of the effect of both the genetic and defocus-induced factors and their interactions in the development of refractive error, while at the

same time maintaining intact the normal accommodative visual feedback control process. The simulation results indicated that genetic factors predominated during the first 15 years, with all refractive groups beginning at a 0.75 D hyperopic refractive error level. There appeared to be three levels of emmetropization in the early years of refractive error development. The HYP group did not exhibit emmetropization, but rather became more hyperopic and eventually leveled off at –1.50 D. After approximately two years, the other three groups emerged from their hyperopic origins. The EMM and LOM groups remained stable at zero refractive error, whereas the EOM group exhibited a continued myopic shift. In contrast to the widespread genetic influence in the refractive groups during the early years, defocus-induced refractive changes occurred after age 15 years, but only in the myopes. This later change was the primary drive in LOM, but it was added as a secondary drive to the genetically-induced change attained earlier in EOM.

Myopia is a complex phenomenon, as it involves the interplay between genetic and environmental factors (3, 42). The genetic influence in EOM was modeled as the continued growth in axial length in excess of that needed for emmetropia (43). The growth rate declined until the axial length attained a fixed level by approximately 15 years of age. The retinal-induced influence was responsible for myopia development in both LOM and EOM after 15 years of age. This is important because myopia affects 25% of the adult population in the United States (44) (with approximately one-third of these being LOM (44, 45)), and at least 75% of the population in Asian countries such as Taiwan (46). The susceptibility to retinal defocus was modeled in terms of the threshold for inducing an axial length change, wherein the thresholds were lower for the myopes than for the EMM and HYP groups. Once the threshold was exceeded, however, the induced change in axial length occurred quite rapidly, attaining a steady-state level within about 5 to 10 years. This is in agreement with clinical and epidemiological research findings (33, 47, 48).

In contrast to myopia and its progressive nature, the refractive condition of hyperopia exhibited a relative insusceptibility to such change in many children and young adults. First, during the initial years of life (ages 1–7 years), hyperopia is the population norm and remains quite stable (31–34); it averaged about 1.50 D (4, 32) and 2.5–3.5 D (33) assessed without and with cycloplegia, respectively, in infants and very young children. Second, in a study of refractive error changes during the first six years of school, it was found that those children who remained hyperopic during this period had a relative myopic rate of change of only –0.07 D/year (49). Third, rate of refractive error change in young myopes was about 2–10 times (–0.46 to –0.93 D/ yr) greater than in age-matched hyperopes (–0.03 to –0.11 D/yr) (33, 47). Fourth, and related to the above, when school-aged hyperopes made the transition to myopia, their rate of refractive error change increased about 3-fold (i.e., –0.21 D/yr vs. –0.60 D/yr) (47, 48). And, lastly, with regard to nearwork-induce transient myopia, it was found that young-adult myopes were particularly susceptible, whereas the hyperopes were particularly insusceptible (4). Thus, further study of hyperopia may lead to a better understanding of myopia, and furthermore yield insight into possible early pre-myopic clinical intervention.

Emmetropization was seen for "induced" refractive error below 0.5 D. This is consistent with the non-monotonic V-shape of the AE_{rms} versus refractive error curve under the Near paradigm. The underlying reason for this can be seen in Fig. 4B. As the "induced" refractive error is increased from 0 to 0.5 D, AE_{rms} shifts in the opposite direction. This will cause a decrease in axial length (Fig. 6), which is consistent with emmetropization. On the other hand, when the "induced" refractive error is above 0.5 D, which shifts the response to the right side of the non-monotonic V-shaped curve, AE_{rms} shifts in the same direction. This would be consistent with the progressive increase in axial length that lead to myopia (50, 51).

During the early stages of ocular growth, hyperopia is normally present and this results in a "negative" refractive error. This negative refractive error biases the operating point to the left side of the V-shaped AE_{rms} versus refractive error curve. As we have seen in the above simulation findings, this results in emmetropization. On the other hand, as ocular growth continues, the refractive error approaches emmetropia. However, with increased nearwork, the refractive error shifts further to the right to operate on the ascending limb of the V-shaped curve. Myopes, with their greater susceptibility, or lower threshold, would exhibit axial elongation with increased retinal defocus, thus resulting in a progression of myopia. Operation in this higher retinal defocus region would be consistent with an earlier hypothesis by Schaeffel and Howland (16), who proposed that "blur always triggers axial growth". It is also in agreement with a more recent hypothesis by Ong and Ciuffreda (3), who proposed that retinal defocus either due to under- or over-accommodation may result in axial elongation, as pure defocus blur is an even-error signal. That is, it provides magnitude but not directional information (52).

The model has therefore provided a simple yet comprehensive overview of the differential interactive effects of genetic and defocus-induced factors that drive refractive error development in the four refractive groups. It has also provided a quantitative framework for the process of emmetropization. Future work would include the effects of preventive (i.e., bifocals) and therapeutic (i.e., vision therapy) paradigms in the clinical care of young children and adults to prevent the development of myopia.

Acknowledgement

Supported in part by NIH T35 Grant – EY07079 –12.

References

1. Smith MS. *Evolutionary Genetics.* Oxford: Oxford University Press; 272–303.
2. Ong E, Ciuffreda KJ. Nearwork-induced transient myopia – a critical review. *Doc. Ophthalmol.* 1995;91:57–85.
3. Ong E, Ciuffreda KJ. *Accommodation, Nearwork, and Myopia.* Santa Ana, CA: Optometric Extension Program Foundation, Inc; 1997.
4. Ciuffreda KJ, Wallis D. Myopes exhibit increased susceptibility to nearwork-induced transient myopia. *Invest. Ophthalmol. Vis. Sci.* 1998;39:1797–1803.
5. Wallman J. Can myopia be prevented? In *14th Biennial Research to Prevent Blindness Science Writers Seminar in Ophthalmology.* New York, NY: Research to Prevent Blindness; 1997:50–52.
6. Birnbaum MH. *Optometric management of nearpoint vision disorders*, Boston, MA: Butterworth-Heinemann; 1993:303–309.
7. Ciuffreda KJ. Accommodation and its anomalies. In: Charman WN. *Vision and Visual Dysfunction: Visual Optics and Instrumentation*, Vol. 1, London: Macmillan; 1991:231–279.
8. Ciuffreda KJ. Accommodation, pupil, and presbyopia. In: Benjamin WJ. *Borish's Clinical Refraction,* Philadelphia, PA: W. B. Saunders Co; 1998:77–120.
9. Ciuffreda KJ, Kenyon RV. Accommodative vergence and accommodation in normals, amblyopes, and strabismics. In: Schor CM, Ciuffreda, KJ. *Vergence Eye Movements: Basic and Clinical Aspects*, Boston, MA: Butterworths; 1983:101–173.
10. Schaeffel F, Troilo D, Wallman J, Howland HC. Developing eyes that lack accommodation grow to compensate for imposed defocus. *Vis. Neurosci.* 1990;4:177–183.
11. Smith EL, Hung LF, Harwerth RS. Effects of optically induced blur on the refractive status of young monkeys. *Vis. Res.* 1994;34:293–301.
12. Grosvenor T, Flom MC, eds. *Refractive Anomalies - Research and Clinical Applications.* Boston, MA: Butterworth-Heinemann; 1991.
13. Christiansen AM, Wallman J. Evidence that increased scleral growth underlies visual deprivation myopia in chicks. *Invest. Ophthal. Vis. Sci.* 1991;32:2134–2150.
14. Drexler W, Findl O, Schmetterer L, Hitzenberger CK, Fercher AF. Eye elongation during accommodation in humans: differences between emmetropes and myopes. *Invest. Ophthal. Vis. Sci.* 1998;39:2140–2147.
15. Gwiazda J, Thorn F, Bauer J, Held R. Myopic children show insufficient accommodative response to blur. *Invest. Ophthal. Vis. Sci.* 1993a;34:690–694.
16. Schaeffel F, Howland HC. Mathematical model of emmetropization in the chicken, *J. Opt. Soc. Am. A* 1988;5:2080–2086.
17. Medina A. A model of emmetropization, the effect of corrective lenses. *Acta Ophthalmol.* 1987;65:585–571.
18. Flitcroft DI. A model of the contribution of oculomotor and optical factors to emmetropization and myopia. *Vis. Res.* 1998;38:2869–2879.
19. Hung GK, Semmlow JL. Static behavior of accommodation and vergence: computer simulation of an interactive dual-feedback system. *IEEE Trans. Biomed. Engin.* 1980;27:439–447.
20. Hung GK. Adaptation model of accommodation and vergence. *Ophthal. Physiol Opt.* 1992;12:319–326.
21. Hung GK, Ciuffreda KJ, Rosenfield M. Proximal contribution to a linear static model of accommodation and vergence. *Ophthal. Physiol. Opt.* 1996;16:31–41.
22. Blackie CA, Howland HC. Extension of the Flitcroft model of emmetropization: inclusion of pupil size. *Invest. Ophthal. Vis. Sci.* 1998;39 (suppl):S279.
23. Hung GK, Ciuffreda KJ. Adaptation model of nearwork-induced transient myopia. *Ophthal. Physiol. Opt.* In press.
24. McBrien NA, Millodot M. The effect of refractive error on the accommodative response gradient. *Ophthal. Physiol. Opt.* 1986;6:145–149.
25. Hung GK. Techniques in the quantitative analysis of the focusing and binocular fixation systems. In Leondes CT, ed. *Computer Techniques and Biotechnology Systems.* Langhorn, PA: Gordon and Beach; in press.
26. Hung GK, Ciuffreda KJ. Accommodative oscillation can enhance average accommodative response. *IEEE Trans. Sys. Man Cyber.* 1982;12:594–598.
27. Krishnan VV, Stark L. Integral control in accommodation. *Comput. Prog. Biomed.* 1975;4:237–245.
28. Thompson HE. *The Dynamics of Accommodation in Primates.* Ph.D. Dissertation, Berkeley, CA: Univ. of Calif. at Berkeley: 1975.
29. McBrien NA, Millodot M. The relationship between tonic accommodation and refractive error. *Invest. Ophthal. Vis. Sci.* 1987;28:997–1004.
30. Scammon RE, Armstrong EL. On the growth of the human eyeball and optic nerve. *J. Comp Neurol.* 1925;38:165–219.
31. Erhlich DL, Atkinson J, Braddick O., Bobier W, Durden K. Reduction of infant myopia: a longitudinal cyclopegic study. *Vis. Res.* 1995;35:1313–1324.
32. Gwiazda J, Thorn F, Bauer J, Held R. Emmetropization and the progression of manifest refraction in children followed from infancy to puberty. *Clin. Vis. Sci.* 1993b;8: 337–344.
33. Slataper FJ. Age norms of refraction and vision. *Arch. Ophthalmol.* 1950;43;466–481.
34. Rosner J. Hyperopia. In Grosvenor T, Flom MC, eds. *Refractive Anomalies.* Boston, MA: Butterworth-Heinemann; 1991:121–130.
35. Atkinson J, Braddick O, Bobier B, Anker S, Ehrlich D, King J, Watson P, Moore A. Two infant vision screening programmes: prediction and prevention of strabismus and amblyopia from photo- and videorefractive screening. *Eye* 1996;10:189–198.
36. Bennett AG, Rabbetts RB. *Clinical Visual Optics*, Woburn, MA: Butterworth-Heinemann; 1989:75.
37. Sorsby A, Leary GA. A longitudinal study of refraction

and its components during growth. *Med. Res. Council Special Report Series no. 309*. London: Her Majesty's Stationery Office; 1970.
38. Goss DA, Wickham MG. Retinal-image mediated growth as a mechanism for juvenile onset myopia and for emmetropization. *Doc. Ophthalmol.* 1995;90,341–375.
39. Grosvenor T, Goss DA. *Clinical Management of Myopia*. Boston, MA: Butterworth-Heinemann; 1999.
40. Hung GK. Sensitivity analysis of the stimulus-response function of a static nonlinear accommodation model. *IEEE Trans. Biomed. Engin.* 1998;45:335–341.
41. Ingram RM, Arnold PE, Dally S, Lucas J. Emmetropization, squint, and reduced visual acuity after treatment. *Brit. J. Ophthalmol.* 1991;75:414–416.
42. Rosenfield M, Gilmartin B. Myopia and nearwork: causation or merely association? In Rosenfield M, Gilmartin B, eds. *Myopia and Nearwork*. Oxford: Butterworth-Heinemann; 1998:193–206.
43. Goldschmidt E. On the etiology of myopia - and epidemiological study. *Acta Ophthalmol.* 1968;98 (suppl):1–72.
44. Sperduto RD, Seigel D, Roberts J, Rowland M. Prevalence of myopia in the United States. *Arch. Ophthalmol.* 1983;101:405–407.
45. Grosvenor T. A review and a suggested classification system for myopia on the basis of age-related prevalence and age of onset. *Am. J. Optom. Physiol. Opt.* 1987;64: 545–554.
46. Lin LLK, Shih YF, Lee YC, Hung PT, Hou PK. Changes in ocular refraction and its components among medical students – a 5-year longitudinal study. *Optom. Vis. Sci.* 1996;73:495–498.
47. Mantyjarvi MI. Changes of refraction in school children. *Arch. Ophthal.* 1985;103:790–792.
48. Hofstetter HW. Some interrelationships of age, refraction, and rate of refractive change. *Am. J. Optom. Arch. Am. Acad. Optom.* 1954;31:161–169.
49. Hirsch MJ. Relationship between refraction and entering school and rate of change during the first six years of school: an interim report from the Ojai Longitudinal Study. *Am. J. Optom. Arch. Am. Acad. Optom.* 1962;39: 51–59.
50. Jiang BC, Woessner WM. Increase in axial length is responsible for late-onset myopia. *Optom. Vis. Sci.* 1996;73:231–234.
51. Siegwart JT Jr, Norton TT. Regulation of the mechanical properties of tree shrew sclera by the visual environment. *Vis. Res.* 1999; 39:387–407.
52. Stark L. *Neurological Control Systems, Studies in Bioengineering*. New York: Plenum Press; 1968:205–219.